Acoustically assisted fibrous filtration for enhanced particle capture

Sudharshan Anandan [1], Andres Barrio-Zhang [1], Akshay Deolia [1], Tyler Hughes [1], Sohum Sodhi [1], Jae Hong Park[2], Ryan Wagner [1], Arezoo Ardekani [1], and David M. Warsinger [1].

[1] School of Mechanical Engineering, Purdue University, West Lafayette, IN 47907, USA
[2] School of Health Sciences, Purdue University, West Lafayette, IN 47907, USA

Abstract. Fibrous filters in air conditioning systems separate particles from the air stream by capturing them on fibers. However, particles in the 0.1–1 µm range, known as the most penetrating particle sizes (MPPS), are difficult to capture because diffusion, interception, impaction, electrostatic, and gravitational forces are not effective at moving these particles toward the fibers. In this work, we demonstrate, through experiments and scaling analysis, that an acoustic standing wave generates two force fields within a fibrous filter. Acoustic interaction forces attract particles to the fibers. Acoustic streaming forms localized mini-vortices near fiber boundaries, increasing the likelihood of particle deposition through fluid drag.Our prior simulation results also showed that acoustic interactions and streaming forces increase particle capture more than particle agglomeration. Agglomeration occurs only at very high concentrations (> 10^5–10^6 particles/cm^3) for submicron aerosols. To determine capture efficiency (η), we conducted experiments in a bench-scale setup. This setup included an aerosol generation subsystem, an acoustically assisted fibrous filtration module, and sampling devices with optical and scanning mobility particle sizers. The sound pressure level inside the acoustic cavity was measured at 1533 Pa. We tested different fibrous filter combinations, varying in filter materials, fiber diameters, porosities, and loading. Here, we present the increase in η of a sintered metallic fiber with a mean fiber diameter of 6.92±2.22 µm as the filter loading increased. For a monodisperse 0.3 µm particle at a filter face velocity of 0.3 m/s,under acoustic excitation, the capture efficiency remained about 40%. Without acoustic assistance, η decreased from about 40% to 27%. These results show that adding acoustic fields to fibrous filtration can greatly enhance particle capture, particularly for the MPPS. This suggests a promising strategy to improve indoor air quality and reduce exposure to airborne contaminants.

Keywords. Acoustic interaction force, Acoustic streaming, Fibrous filters, Filter loading

1 Introduction

Indoor air pollution is the third leading cause of death, according to the World Health Organization (WHO) report released in 2021[1]. The United States Environmental Protection Agency (EPA) reported that humans spend 80% of their time indoors, and this is expected to increase further [2]. Given the increased levels of indoor air pollution, the current fibrous filters used in the ventilation systems or air conditioning systems poorly capture the particle sizes ranging from 0.1–1 µm also known as the most penetrating particle sizes (MPPS) [3]. Current fibrous filters rely on passive transport mechanisms such as diffusion, gravitational settling, interception, and impaction to trap the particles flowing through a fibrous filter medium [4] . However, this passive transport does not effectively manipulate the particle toward the fibrous filters. Current filtration technologies, especially higher minimum efficiency reporting value (MERV) — a metric used to quantify the capture efficiency of the filters — rely on either electrostatic forces as an active mechanism for particle capture or denser filters that cause a larger pressure drop. The capture efficiency of the electrostatic filters decreases over time as particles already deposited on the filters reduce the electrostatic attraction[5].

In this study, we explored an active mechanism using an acoustic field in combination with fibrous filters to enhance the capture efficiency at the MPPS. Specifically, this study demonstrates that the use of standing acoustic waves with a fibrous filter results in two force fields: acoustic interaction forces and streaming that enhance the capture of the MPPS particles by actively manipulating the particles towards the fiber surfaces[6]. Prior studies attributed the increase in filter capture efficiency to particle agglomeration[7], without focusing on fiber-particle interactions, whereas this study demonstrates that the fiber-particle interactions are more dominant than the inter-particle interactions upstream of the fiber filter.

Another important aspect of acoustically aided filtration is the extended filter lifetime. The lifetime extension occurs because of non-uniform particle loading—which disperses particles unevenly across the filter surface—and the dendritic formation of particles that build branched particle clusters deeper within the filter, both of which reduce upstream clogging [8,9]. Studies show that acoustic components consume less energy than the fan power required to compensate for the pressure drop caused by clogged filters [8,10]. Multiple factors impact the acoustically activated capture mechanisms: fiber diameter, filter medium porosity, Young's modulus of the filter material, particle size, flow velocity, acoustic pressure inside the channel, frequency of the acoustic wave, and filter loading. In this work, we specifically investigated how particle loading affects the capture efficiency of sintered metal fibrous filters.

2 Background and Theory

2.1 Passive Filtration Mechanisms

Fibrous filters, in the absence of an acoustic field, rely on passive filtration mechanisms, including interception, impaction, diffusion, gravitational settling, and electrostatic attraction. The dominant mechanism depends strongly on particle size, flow velocity, and fiber diameter. Diffusion — random motion of particles due to the constant bombardment of air molecules— is a dominant form of capture for ultrafine particles (0.01–0.1 µm) [4] and starts to decay drastically with an increase in particle size. For the MPPS range, it largely depends on interception — particles intercepted by the filter fibers when they follow streamlines and flow over the fibers — and diffusion. When particles or fibers are charged, electrostatic attraction also plays a dominant role in their capture. In this study, where a charged particle approaches a conductive fiber, the electrostatic image force becomes dominant in the vicinity of the fiber[11]. Inertial impaction is the main mode of capture for larger particles 2–10 µm [4].

Acoustically Activated Filtration Mechanism

Fig. 1 illustrates the formation of an acoustic standing wave inside a parallel-plate channel. In this half-wave resonator, sound emitted by the acoustic actuator reflects from the opposite wall and overlaps with the incoming wave. This interference creates a standing-wave pattern in the y-direction, characterized by alternating antinodes (regions of maximum pressure) at the actuator and reflector walls, and a node (region of minimum pressure) at the channel center. The resulting spatially fixed pressure and velocity fields interact with suspended particles and the fibrous medium, giving rise to three important effects: primary and secondary acoustic radiation forces, and acoustic streaming.

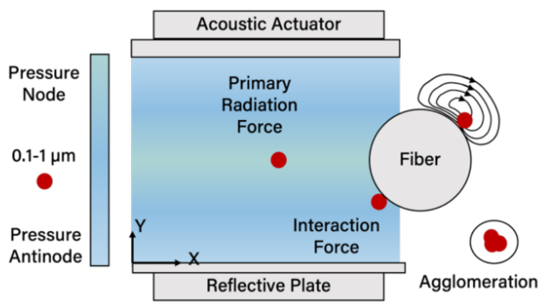

Fig. 1. Illustration of a standing acoustic wave in a 2D parallel plate channel showing the acoustical force on the particle and fiber

The primary acoustic radiation force is the time-averaged net force acting on an individual particle due to acoustic pressure and velocity gradients. Its magnitude and direction depend on the particle-fluid density and compressibility contrasts, and it tends to drive particles toward either pressure nodes or antinodes. The secondary acoustic radiation force arises from the interaction of scattered acoustic fields between particles and between particles and nearby boundaries (e.g., fibers). These forces can be attractive or repulsive. For 0.3 µm particles, high particle number concentrations (on the order of 10^6 particles/cm^3 or higher[12] , are required for secondary forces to promote particle-particle interactions and agglomeration. At dilute concentrations, the dominant effect in our configuration is a particle-fiber interaction force that attracts particles toward the fiber surface, effectively enhancing particle-filter collisions.

Finally, acoustic streaming is a steady, vortical flow generated by viscous attenuation of the oscillatory sound field near solid boundaries. Around the fibers, this streaming induces localized mini-vortices that create additional fluid drag on particles and increase the particle transport across the streamlines, thereby raising the probability that particles are brought into contact with the fibers.

3 Materials and Methods

3.1 Experimental Setup

This section describes the critical components of the bench-scale setup. As shown in Fig. 2, the bench-scale setup consisted of four major subsystems: (1) clean-air subsystem, (2) aerosol generation subsystem, (3) acoustics subsystem, and (4) sampling subsystem. The clean-air system utilized a pressurized nitrogen (N_2) source, which then passed through a regulator and a high-efficiency particulate air (HEPA) filter (Pall HEPA Capsule filter) to remove background particles, providing a stream of air that carries only aerosolized particles.

Once the clean air was supplied, it flowed through a manifold to provide multiple air streams to the setup. The stream was then split into two streams using two mass flow controllers (MFCs), with MFC 1 supplying the main flow stream to the channel and MFC 2 supplying the aerosolized particles. The aerosol generation systems comprised a vibrating-mesh nebulizer (Aerogen Solo) and a custom-made diffusion dryer. The airstream from the MFC 2 carried the aerosolized polystyrene spheres to the mixing chamber via the diffusion dryer—the desiccant adsorbs unwanted small-sized liquid aerosols, providing a monodisperse size distribution. The mixing chamber was used to increase particle residence time, resulting in a well-mixed airstream at the inlet of the acoustical duct setup.

The acoustical module consisted of two parallel plates: the bottom plate mounts the acoustic transducer (SensComp Series 600 Open Face Ultrasonic Transducer #604150), and the top plate serves as a reflector to generate standing

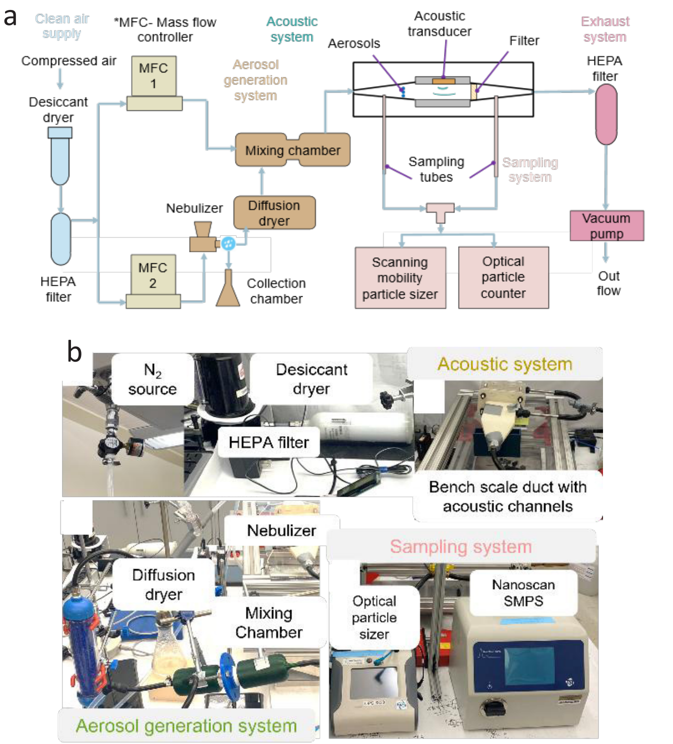

acoustic waves. The dimensions of the channel are 43.5 mm length (x-direction), a height of 3.43 mm in the y-

Fig. 2. (a) Schematic of the bench-scale filtration setup (b) Photos of the actual bench-scale filtration setup

direction and 63.4 mm width that goes into the page in z-direction. The porous media, in this case a fiber filter, was placed as close as possible to the acoustic transducer to exploit the acoustic interaction effects. Furthermore, the sampling system consisted of stainless steel tubes to prevent electrostatic charge buildup, which can increase the likelihood of particle deposition and lead to sampling inaccuracies. To monitor particle size distribution, we used two particle sizers in the system, namely the Optical Particle Sizer (OPS; TSI OPS 3330) and the Scanning Mobility Particle Sizer (SMPS; NanoScan SMPS 3910). The OPS measured the particle's optical diameter, and the SMPS measures the particle's electrical mobility diameter. Table 1 presents the experimental conditions used in the study.

Table 1 – **Experimental conditions**

Parameters	Units	Values
Face velocity (u)	m/s	0.3
Frequency (f)	kHz	44.8
Seeding particle (d_p)	µm	0.3

3.2 Aerosol Characterization and Capture Efficiency Measurements

We used 0.3 µm polystyrene microspheres as the seeding particles in a deionized water suspension and aerosolized them using the vibrating-mesh nebulizer. Particle size statistics used in this study considered the measurements only from the OPS. The geometric standard deviation (GSD) and the count median diameter (CMD) were measured as 1.20±0.003 and 0.38±0.003 µm, respectively. These values confirm that the particle size distribution (PSD) was monodisperse. While the absolute upstream particle concentrations varied from ~4000–5500 particles/cm^3 throughout the experimental trials due to nebulizer mesh fouling, the GSD and CMD remained invariant.

Capture efficiency was determined by measuring the downstream particle concentration (C_{down}) and a time-synchronized upstream reference concentration (C_{up}) as suggested by the ASHRAE 52.2 standards [13]. The upstream concentration for a specific downstream sampling point t_i was calculated by averaging the upstream concentration from the preceding (t_{i-1}) and succeeding (t_{i+1}) sampling intervals.

$$\eta = 1 - \frac{C_{down}}{C_{up}}. \quad (1)$$

3.3 Filter Characterization

The filtration media used in this study were random sintered metal fibrous filters made of 316L stainless steel (Xiamen Zopin New Materials Limited) with a porosity (α) of 0.75±0.1. The filter was characterized by scanning electron microscopy (SEM;Teneo Volumescope), as shown in Fig. 3. The fiber diameter distribution was then analyzed using image processing software (ImageJ), yielding a mean diameter (d_f) of 6.92±2.22 µm. Unlike the flexible polymeric filters, the stainless steel fibers are rigid structures. When subjected to a high-pressure standing wave, these fibers act as more effective scatterers, which enhances acoustic interaction and promotes particle capture around the fibers.

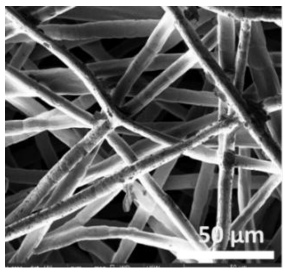

Fig. 3. Scanning electron microscopy (SEM) image of a random sintered fibrous metal filter

3.4 Acoustic Field Characteristics

The SensComp electrostatic transducer is driven using a ~170V_{peak} sine wave with a ~170 V_{DC} offset generated using a function generator (Tektronix AFG1062) and an amplifier (Trek PZD350A). A 4V_{peak} sine wave offset with 2V_{DC} was fed as an input signal from the function generator into the amplifier. The input gain screw on the front panel of the amplifier was turned until ~170 V_{peak} and ~170 V_{DC} offset was obtained across the transducer's leads. The microphone output was measured using a Picoscope 4224 oscilloscope and a prepolarized free field microphone (GRAS 40BE) with applied pressure correction. Fig. 4 shows the linear chirp frequency sweep of the acoustic cavity from 40–60 kHz, with a dominant resonance at ~46.5 kHz (f_0) and a peak pressure amplitude of 1533 Pa. This pressure amplitude corresponds to a sound pressure level (SPL) of ~157dB. While this magnitude is high, the system operates at an ultrasonic frequency of 46.5kHz, well above the human audible range (<20 kHz), ensuring silent, safe operation in occupied spaces. Furthermore, the quality factor of the acoustic cavity is estimated to be 13 using the half-power criterion (Q≈ $\omega_0/\Delta\omega$), where ω is the angular frequency of the acoustic wave and ω_0 is the resonant frequency.

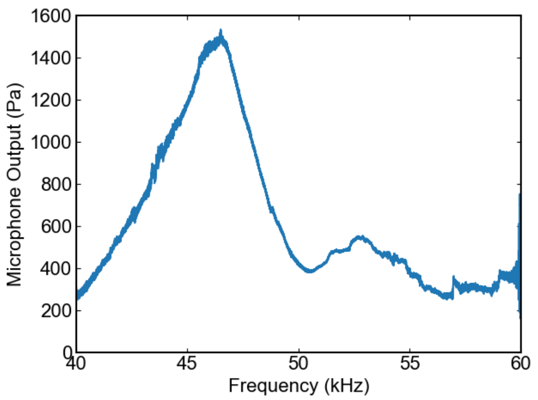

Fig. 4. Pressure measurement inside the channel

3.5 Theoretical Framework and Mechanistic Scaling Analysis

We performed a mechanistic scaling analysis as a guide to explain the experimental results. Using measured parameters, the dominant forces acting on a 0.3 µm particle were estimated. This approach linked capture efficiency to the acoustic field, highlighting the influence of acoustic versus passive forces.

3.5.1 Single Fiber Filtration Efficiency Models

The current study used the single-fiber filtration efficiency models (SFFE) [4] and assumed that the total capture efficiency equals the sum of the capture efficiencies from independent mechanisms as given by Eq. (2).

$$\eta_{total} = \eta_R + \eta_I + \eta_D + \eta_E + \eta_A \tag{2}$$

where η_{total} is the total capture efficiency, η_I is the capture efficiency due to interception, η_D is the capture efficiency due to diffusion, η_E is the capture efficiency due to electrostatic image force, and η_A is the capture efficiency due to the acoustical interactions with the fiber filter. We computed the single-fiber filtration efficiencies for different mechanism using the expressions provided in Table 2.

Table 2 – **Summary of capture efficiency expressions**

Mechanism	Expression	Reference
Interception	$\eta_R = \dfrac{(1-\alpha)\left({d_p}/{d_f}\right)^2}{Ku\left(1+{d_p}/{d_f}\right)}$ $Ku = \left(\dfrac{-\ln\alpha}{2} - \dfrac{3}{4} + \alpha - \dfrac{\alpha^2}{4}\right)$	[4]
Inertial Impaction	$\eta_I = \dfrac{Stk^3}{Stk^3 + 0.77Stk^2 + 0.22}$ $Stk = \dfrac{C_c\rho_p u d_p^2}{18\mu d_f}$	[14]
Diffusion	$\eta_D = 2\,Pe^{-2/3}$ $Pe = \frac{d_f u}{D}$; $D = \frac{kTC_c}{3\pi\mu d_p}$	[15]
Electrostatic Image	$\eta_E = \beta\sqrt{K_{IM}}$ $K_{IM} = \left(\dfrac{\varepsilon_f - 1}{\varepsilon_f + 2}\right)\dfrac{C_c n^2 e^2}{12\pi^2\mu u\varepsilon_0 d_p d_f^2}$	[16]

Inertial impaction depends on the particle's Stokes number (Stk), which describes how well the particle follows the fluid streamlines. The expression for Stokes also takes into account the particle slip using the Cunningham slip correction factor (C_c). Since Stk<<1 for the given particle size and velocity, we neglected the inertial impaction.

The SFFE expression for diffusion considers the Peclet number (Pe), which defines the ratio of convective transport along the fiber to the diffusive transport, computed from the particle's diffusion coefficient (D). The diffusion coefficient is further calculated using k (Boltzmann constant), temperature T and the diameter of the particle . On the other hand, the interception of the particle is mainy defined by the ratio of particle diameter (d_p) to the particle fiber diameter (d_f) and the Kuwabara factor (Ku) ,which is a function of the porosity(α). Both diffusion and interception contribute on the same order ~0.5–0.7%. Electrostatic attraction due to the image force is also on the same order of ~0.5–0.7% for the given operating conditions. The dimensionless image force number (K_{IM}) accounts for the particle's charge. This charge is given by the product of the number of elementary charges (n) , assumed to be 5 in this case [17] , and e=1.6×10^{-19} C. Furthermore, ε_{f} is the dielectric constant of the fiber that changes as the experiment progresses. The efficiencies reported from the SFFE expressions are for a single fiber; the overall efficiency is higher due to multiple fibers and the change in filter porosity with increasing filter loading.

3.5.2 Acoustic Transport and Deposition Scaling

Fibrous filters, when exposed to acoustical standing waves, can increase capture efficiency through three main mechanisms: the primary radiation force, the interaction force, and the acoustic streaming-induced drag force, which pushes particles toward the fiber. Notably, the acoustic boundary layer thickness ($\delta = \sqrt{\frac{2\nu}{\omega}}$) , where ν is the kinematic viscosity of air and ω is the angular frequency of the acoustic wave, is 10 μm, which is comparable to the fiber diameter and larger than the particle diameter; thus, the near field effects become more dominant. To clarify these effects, we performed a scaling analysis of the different acoustic forces. Table 3 presents the scaling expressions for the considered acoustic forces.

Table 3 – **Scaling expressions for different acoustic forces**

Mechanism	Force scaling expression	Reference
Primary radiation force	$F_{rad} \propto \mathrm{A}\, k\, p_a^2\, \rho\, c^{-2}\, r_p^3$	[18]
Interaction force	$F_{int} \propto \frac{r_p^6}{d^4}\, \rho\, v_{ac}^2$ $v_{ac} = \frac{p_a}{\rho c}$	[19]
Streaming induced drag	$F_{str-drag} \propto \mu\, u_s.\, r_p$ $u_s \approx \frac{3v_{ac}^2}{4\omega d_f}$	[20,21]

The force expressions in the table apply to an ideal fluid. We recognize the limitations of using an ideal theory, as the relevant length scales—particle, fiber, and viscous boundary thickness—are comparable, and a thermoviscous model should ideally be considered. As established in prior sections, the dominant forces in the passive condition are diffusion, interception, and image force attraction. During passive filtration, the filter's porosity and the ratio of particle to the filter diameter determine whether particles are intercepted by the fibers.

The flow drags the particles in the x-direction, and the convective flow drag typically scales to about 10^{-11} N. If all forces are insufficient or there is no physical interception, particles escape and penetrate the filter. The diffusive force ($\sim k$ T/d_p [22]) is about 10^{-14} N and the electrostatic image force ($\sim q/\varepsilon_0 d^2$ [11]) ranges from 10^{-11}–10^{-19} N, depending on charge, separation distance, and dielectric constant. We next describe the relevant forces in an active acoustic field to contrast them with passive mechanisms.

When the acoustic field is activated, the primary radiation force on 0.3 μm particles is about 10^{-17} N (at ~1500 Pa peak pressure). Secondary (particle-particle) radiation forces vary widely, from 10^{-7}–10^{-20} N, over a 300–1500 Pa pressure amplitude and a 10 nm to 10 μm separation, with the filter face pressure estimated at 300 Pa in a preliminary COMSOL Multiphysics model. Streaming-induced drag force, approximately 10^{-11} N, is of similar magnitude to the passive convective drag. This analysis suggests that, compared to the passive regime, acoustically induced streaming drag can more effectively pull particles toward fibers, while acoustic interaction forces can exceed passive image forces in the immediate vicinity of the fiber. This highlights how acoustics can dominate particle capture under specified conditions, as seen in previous device studies[23].

4 Results and Discussion

4.1 Acoustically Enhanced Capture and Loading Performance

Fig. 5 shows the capture efficiency of the fibrous filter over continuous operation time. Under acoustics ON conditions, the capture efficiency remained ~40%, whereas η decreased from ~40% to 27%. This difference can be explained by observing the changes in the filter's properties,especially,K_{IM}.

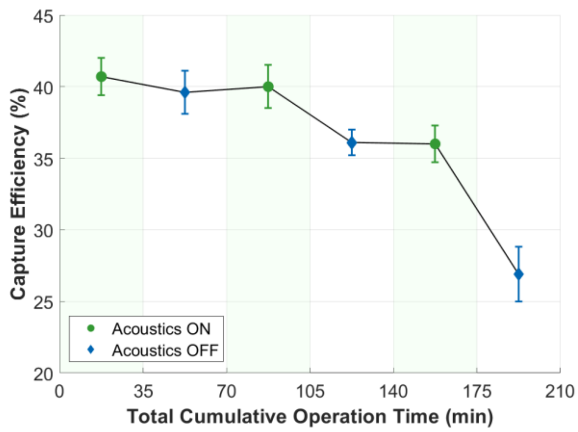

Fig. 5. Capture efficiency under acoustic ON and OFF conditions

Initially, when the filter loading is minimum, the dielectric constant(ε_f) for the fiber is infinity, since it is a conductive fiber and is likely to attract more particles.The decrease in capture efficiency may be explained by the deposition of polystyrene spheres reducing the dielectric constant of the fibers [23]. However, when the acoustic field is applied, the scaling analysis from our prior sections indicates the contribution of strong acoustic induced forces promote particle deposition on the fibers.

4.2 Absence of Agglomeration: Unchanged Particle Size Distribution

Fig. 6 clearly illustrates that there is no particle agglomeration for the submicron particles. The scaling analysis strongly suggests that the interparticle attraction is four to five orders of magnitude lower than the other forces when the separation distance is 10 µm. For the particle concentrations considered in this study,the average inter-particle separation distance can be given as ($d = C^{-1/3}$) ~400 µm . This suggests that inter-particle interactions would be minimal and hence no agglomeration. However, close to the fiber, streaming and interaction forces can synergistically enhance particle capture.

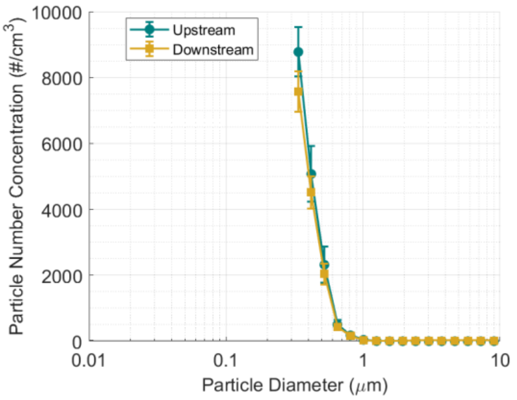

Fig. 6. Particle concentration and upstream and downstream of the acoustic cavity under acoustic ON conditions without the presence of the filter.

4.3 Physical Evidence of Sub-micron Particle Clusters

Fig. 7 presents an SEM image illustrating dendritic particle accumulation on metallic fiber surfaces. According to oscillatory flow theory around cylinders, vortex direction drives particles toward the fiber[21]. Furthermore, from the scaling analysis, the most likely explanation is that the streaming drag pushes the particles toward the fibers, and once they are in the vicinity of the fibers, the interaction force from the already deposited particles may attract them, forming particle clusters. This mechanism likely explains the observed particle clustering around the fibers, as supported by SEM images. Additionally, Moldvasky et al. [9] reported that previously deposited particles promote dendritic formation. Their study demonstrates that such deposits generate streaming vortices, guiding incoming particles toward these sites and forming a porous cake layer that gradually decreases the pressure drop across the filter.

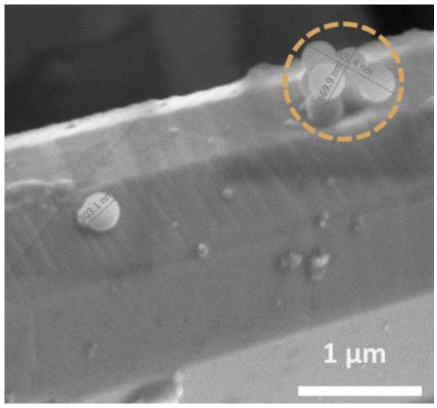

Fig. 7. SEM image showing sub-micron particles deposited on the sintered metallic fibers; orange dashed circle shows the dendritic particle formation

5 Conclusion

This work explores the use of a standing acoustic wave field with a stainless steel fibrous filter and its impact on the filter's long-term performance. For 0.3 µm monodisperse particles, η dropped from ~40% to 27% without acoustics, but remained at ~40% with acoustics. To further analyze these effects, we performed a scaling analysis using a single-fiber efficiency model, which showed that interception, diffusion, and image force contributed equally to η, while image force decayed with filter loading. As the filter operation continued and more particles deposited on the fiber, particle capture by image force decreased. However, with acoustics, the interaction between the standing wave and the fiber filter sustained particle capture over longer periods of time.

Therefore, our results demonstrate that with acoustics, the standing-wave field maintains higher particle capture via acoustically induced effects, offsetting the lack of electrostatic attraction. Given that some higher MERV-rated (13 and above) filters use electrostatically charged media, implementing an active filtration technique is essential for sustaining high capture efficiency over extended periods. Ultrasonic frequencies above the human audible range (>20kHz) enable safe, silent operation in residential and commercial spaces. For large-scale applications, an array of acoustic transducers can be integrated to form a larger duct-based system, similar to that described in Nelson [24]. However, the placement of the filter must be carefully considered to maximize filtration improvements. As mentioned earlier, the use of acoustics increases filter lifetime and provides long-term energy savings. Future work aims to measure filter pressure drop and efficiency with and without acoustics. This will quantify the improvements from acoustics and analyze energy savings, including power consumption, compared to long-term energy savings from fan energy use.

Acknowledgements

This research was supported by the Purdue University Centre for High-Performance Buildings (CHPB-64-2023-25). Furthermore, the authors would especially like to thank Fabian Jahnig and Roman Kappeler from Belimo for their continued suggestions and support throughout the project.

References

[1] "Household Air Pollution." [Online]. Available: https://www.who.int/news-room/fact-sheets/detail/household-air-pollution-and-health. [Accessed: 10-Jan-2026].

[2] US EPA, O., 2017, "Indoor Air Quality." [Online]. Available: https://www.epa.gov/report-environment/indoor-air-quality. [Accessed: 10-Jan-2026].

[3] Kowalski, W. J., Bahnfleth, W. P., and Carey, D. D., 2002, "Engineering Control of Airborne Disease Transmission in Animal Laboratories," Contemp. Top. Lab. Anim. Sci., **41**(3), pp. 9–17.

[4] Hinds, W. C., 1999, *Aerosol Technology: Properties, Behavior, and Measurement of Airborne Particles*, Wiley-Interscience.

[5] He, W., Zhao, Y.-B., Jiang, F., Guo, Y., Gao, H., Liu, J., and Wang, J., 2020, "Filtration Performance and Charge Degradation during Particle Loading and Reusability of Charged PTFE Needle Felt Filters," Sep. Purif. Technol., **233**, p. 116003. https://doi.org/10.1016/j.seppur.2019.116003.

[6] Barrio-Zhang, A., Anandan, S., Deolia, A., Wagner, R., Warsinger, D. M., and Ardekani, A. M., 2024, "Acoustically Enhanced Porous Media Enables Dramatic Improvements in Filtration Performance," Sep. Purif. Technol., **342**, p. 126972. https://doi.org/10.1016/j.seppur.2024.126972.

[7] Ng, B. F., Xiong, J. W., and Wan, M. P., 2017, "Application of Acoustic Agglomeration to Enhance Air Filtration Efficiency in Air-Conditioning and Mechanical Ventilation (ACMV) Systems," PLoS ONE, **12**(6), pp. 1–26. https://doi.org/10.1371/journal.pone.0178851.

[8] Zhang, X., Liu, P., Liu, G., Lim, S. H., Yin, H., Wan, M. P., Lisak, G., and Ng, B. F., 2025, "Maximizing Aerosol Filtration *via* Acoustics," J. Hazard. Mater., **496**, p. 139503. https://doi.org/10.1016/j.jhazmat.2025.139503.

[9] Moldavsky, L., Fichman, M., and Gutfinger, C., 2006, "Enhancing the Performance of Fibrous Filters by Means of Acoustic Waves," J. Aerosol Sci., **37**(4), pp. 528–539. https://doi.org/10.1016/j.jaerosci.2005.05.004.

[10] Liu, P., Zhang, X., Liu, G., Hao Lim, S., Pun Wan, M., Lisak, G., and Feng Ng, B., 2024, "Ultrasonic Aerosol Agglomeration: Manipulation of Particle Deposition and Its Impact on Air Filter Pressure Drop," Ultrason. Sonochem., **103**, p. 106774. https://doi.org/10.1016/j.ultsonch.2024.106774.

[11] Sayoud, M. A., and Zouzou, N., 2025, "Effect of Particle Electrostatic Charge Level on Collection Efficiency of an Electric Metal Mesh Filter," J. Electrost., **138**, p. 104159. https://doi.org/10.1016/j.elstat.2025.104159.

[12] Yan, J., Chen, L., and Li, Z., 2016, "Removal of Fine Particles from Coal Combustion in the Combined Effect of Acoustic Agglomeration and Seed Droplets with Wetting Agent," Fuel, **165**, pp. 316–323. https://doi.org/10.1016/j.fuel.2015.10.077.

[13] ANSI/ASHRAE, 2017, "ANSI/ASHRAE Standard 52.2-2017, Method of Testing General Ventilation Air-Cleaning Devices for Removal Efficiency by Particle Size," ASHRAE Stand., **2017**(STANDARD 52.2), pp. 1–64.

[14] "Landahl, H. D. and Hermann, R. G. (1949) Sampling of Liquid Aerosols by Wires, Cylinders and Slides, and the Efficiency of Impaction of Droplets, J. Coll. Sci., 4, 103-136."

[15] "Kirsch, A. A. and Fuchs, N. A. (1968) Studies of Fibrous Aerosol Filters - III. Diffusional Deposition of Aerosols in Fibrous Filters, Ann. Occ. Hyg., 11, 299-304."

[16] Alonso, M., Alguacil, F. J., Santos, J. P., Jidenko, N., and Borra, J. P., 2007, "Deposition of Ultrafine Aerosol Particles on Wire Screens by Simultaneous Diffusion and Image Force," J. Aerosol Sci., **38**(12), pp. 1230–1239. https://doi.org/10.1016/j.jaerosci.2007.09.004.

[17] Chen, H., Zhang, Z., Zhang, Z., Jiang, F., and Du, R., 2018, "Enhancement of Filtration Efficiency by Electrical Charges on Nebulized Particles," Particuology, **37**, pp. 81–90. https://doi.org/10.1016/j.partic.2017.07.008.

[18] Imani, R. J., and and Robert, E., 2018, "Estimation of Acoustic Forces on Submicron Aerosol Particles in a Standing Wave Field," Aerosol Sci. Technol., **52**(1), pp. 57–68. https://doi.org/10.1080/02786826.2017.1383968.

[19] Silva, G. T., and Bruus, H., 2014, "Acoustic Interaction Forces between Small Particles in an Ideal Fluid," Phys. Rev. E, **90**(6), p. 063007. https://doi.org/10.1103/PhysRevE.90.063007.

[20] Muller, P. B., Barnkob, R., Jensen, M. J. H., and Bruus, H., 2012, "A Numerical Study of Microparticle Acoustophoresis Driven by Acoustic Radiation Forces and Streaming-Induced Drag Forces," Lab. Chip, **12**(22), pp. 4617–4627. https://doi.org/10.1039/C2LC40612H.

[21] Schlichting, H., and Gersten, K., 2017, *Boundary-Layer Theory*, Springer, Berlin, Heidelberg. https://doi.org/10.1007/978-3-662-52919-5.

[22] Sardari, P. T., Rahimzadeh, H., Ahmadi, G., and Giddings, D., 2018, "Nano-Particle Deposition in the Presence of Electric Field," J. Aerosol Sci., **126**, pp. 169–179. https://doi.org/10.1016/j.jaerosci.2018.09.012.

[23] Hammarström, B., Laurell, T., and Nilsson, J., 2012, "Seed Particle-Enabled Acoustic Trapping of Bacteria and Nanoparticles in Continuous Flow Systems," Lab. Chip, **12**(21), pp. 4296–4304. https://doi.org/10.1039/C2LC40697G.

[24] Nelson, A. J., 2011, "Bench-Scale Evaluation of an Energy Efficient Acoustic Aerosol Purification Device with a Newly Designed Bioaerosol Testing and Evaluation Chamber," University of Illinois at Urbana-Champaign.